

Numerical Heat Transfer, Part B: Fundamentals



Date: 05 July 2017, At: 08:07

ISSN: 1040-7790 (Print) 1521-0626 (Online) Journal homepage: http://www.tandfonline.com/loi/unhb20

Heat and Mass Transfer in Moist Soil, Part I. Formulation and Testing

F. Moukalled & Y. Saleh

To cite this article: F. Moukalled & Y. Saleh (2006) Heat and Mass Transfer in Moist Soil, Part I. Formulation and Testing, Numerical Heat Transfer, Part B: Fundamentals, 49:5, 467-486

To link to this article: http://dx.doi.org/10.1080/10407790500510866



Full Terms & Conditions of access and use can be found at http://www.tandfonline.com/action/journalInformation?journalCode=unhb20

Copyright © Taylor & Francis Group, LLC ISSN: 1040-7790 print/1521-0626 online

DOI: 10.1080/10407790500510866



HEAT AND MASS TRANSFER IN MOIST SOIL, PART I. FORMULATION AND TESTING

F. Moukalled and Y. Saleh

Department of Mechanical Engineering, American University of Beirut, Riad El Solh, Beirut, Lebanon

An unsteady two-dimensional model of heat and mass transfer through soil is implemented within a finite-volume-based numerical method. The model follows a phenomenological formulation for the transfer processes with temperature and matric potential (ψ) as the dependent variables. The finite-volume method being inherently conservative, the mass imbalance problem reported in the literature when employing the \psi-based formulation with other numerical methods is prevented. A partial elimination algorithm is applied within the iterative solution procedure to increase its implicitness and improve its robustness. The accuracy of the model is established by solving the following three test problems: temperature distribution in dry soil; moisture distribution in isothermal soil; and coupled heat and water vapor diffusion in soil. Results are presented in the form of temporal profiles of temperature and moisture content and compared against analytical values. Excellent agreement is obtained, with numerical profiles falling on top of theoretical values.

INTRODUCTION

Soil is considered a nonhomogeneous and nonisotropic porous material composed of a mixture of liquid moisture, vapor, and air in the pores. The prediction of moisture and temperature distribution in soil is useful in many applications, such as agriculture, irrigation, heat and moisture transmission between a building and its surrounding, and the detection of buried objects, to cite a few. This work was motivated by the need to develop a numerical tool for the prediction of the surface thermal signature of buried landmines in moist soil, which is the subject of a companion article [1]. In this article the finite-volume-based numerical method that is used in [1] for predicting the heat and moisture distribution in soil with a buried landmine is developed and tested.

In analyzing coupled mass and heat transfer in a porous medium, investigators have followed two macroscopic approaches. The first approach applies the

Received 27 June 2005; accepted 8 November 2005.

The authors gratefully acknowledge the support of the Lebanese National Council for Scientific Research through Grant LCR-11304-002208 and Mr. Youssef Jameel through Grant DCU 113010-024021. Special thanks are due to Prof. Z. Fawaz for initiating this collaborative research project between the American University of Beirut and Ryerson University in Toronto, Canada.

Address correspondence to F. Moukalled, Department of Mechanical Engineering, American University of Beirut, P.O. Box 11-0236, Riad El Solh, Beirut 1107 2020, Lebanon. E-mail: memouk@ aub.edu.lb

NOMENCLATURE			
a_P^{ϕ}, a_F^{ϕ}	coefficients in the discretized		tantuacity factor on cooling factor
u_{P}, u_{F}		Γ	tortuosity factor or scaling factor diffusion coefficient
b_P^{ϕ}	equation for φ source term in the discretized	δ	unit vector in the direction of the
ν_P	equation for ϕ	U	line joining grid points P and F
C	volumetric heat capacity, J/m ³ K	Δt	time step
C_P	specific heat capacity, J/kg K	η	soil porosity
$C_{Tv}, C_{T\psi}$	vapor and total moisture thermal	θ	volumetric moisture content,
$C_{Iv}, C_{I\psi}$	capacitance terms, K ⁻¹	· ·	m ³ /m ³
C^{ϕ}	coefficient in general conservation	Θ	degree of saturation
	equation	к	space vector
$C_{\psi T}, C_{TT}$	matric, J/m^4 , and thermal, $J/m^3 K$,	ξ	temperature gradient ratio
- ψ1 , -11	heat capacitance terms	ρ	density, kg/m ³
$C_{\Psi v}, \ C_{\Psi \Psi}$	matric vapor and total moisture	σ	water surface tension, N/m, and
φνησφ	capacitance terms, m ⁻¹		Stefan-Boltzmann constant,
d	vector joining grid points P and F		$W/m^2 K$
D_a	molecular diffusivity of water vapor	τ	empirical constant used in hydraulic
	in air, m ² /s		conductivity equation
$D_{Tv},D_{T\psi}$	vapor and total moisture thermal	ф	general scalar variable
	diffusivities, m ² /s K	φ	relative humidity
$D_{\psi v},D_{\psi \psi}$	matric vapor and total moisture	Φ	total soil matric potential for liquid
	diffusivities, m/s		flow, m
$D_{\psi T}$	matric potential heat diffusivity,	ψ	matric liquid potential (pressure
	W/m^2		head), m
f(), f	correction and interpolation factor; also refers to <i>e</i> , <i>w</i> , <i>n</i> , or <i>s</i> face of	Ω_P	volume of cell P
	control volume P	6.1	
F	refers to the E , W , N , or S neighbor	Subscripts	ambient air
1	of grid point P	a £	refers to control-volume face
g	gravitational acceleration, m/s ²	F	
g_i	shape factors used in estimating soil	r k	refers to grid point <i>F</i> critical
31	thermal conductivity	1	liquid
h	convective heat transfer coefficient,	nb	refers to values at the faces obtained
	$W/m^2 K$	по	by interpolation between <i>P</i> and its
h_{fg}	latent heat of vaporization of water,		neighbors
78	J/kg	NB	refers to neighbors of
K	hydraulic conductivity of soil, m/s		grid point P
k, k^*	effective and dry soil thermal	0	reference value
	conductivity, W/m K	P	refers to the grid point P
n	unit vector in the S direction	r	residual or reference
P	main grid point	S	saturated, surface
q'''	heat generation, W/m ³	v	vapor
Q^{ϕ}	source term in general conservation	vs	saturated vapor
	equation	W	water, wind
R_w	gas constant for water vapor, J/kg K		
\mathbf{S}_f	surface vector	Superscripts	
t T	time, s	D	refers to diffusion contribution
T	temperature, K	(n - 1)	refers to values from the previous
u_l	bulk liquid velocity, m/s		iteration
Z	vertical distance, m	t o	refers to transient contribution
α	fitting parameter for moisture	-	refers to values from the previous
	retention curve, m ⁻¹ , or underrelaxation factor		time step
	underrelaxation factor	_	refers to an interpolated value

thermodynamics of irreversible processes to describe the interaction of the forces and fluxes involved [2]. The second technique, adopted in this work, is based on the phenomenological processes that occur in soil [3–5]. The phenomenological formulation of transfer mechanisms in soil began with the work of Philip and de Vries [3], who discussed liquid and vapor transfer in a porous medium under the effects of temperature and moisture content gradients. They presented a heat conduction equation that incorporated latent heat transfer by vapor diffusion. De Vries [4] later generalized these equations by taking into account moisture and latent heat storage in the vapor phase, heat of wetting, and sensible heat transfer by liquid movement. Sophocleous [6] converted Philip and de Vries' θ -based equations [3], θ being the volumetric moisture content, into a matric head (ψ)-based formulation. Milly [5] showed that Sophocleous's system of equations was incorrectly formulated, with major theoretical errors in the equation for the liquid flux and in the expression for the temperature dependence of matric potential, and reconverted the equations of de Vries [4] to the ψ-based formulation. Recently, Deru [7] and Janssen [8] used a similar model to study the influence of soil moisture transfer on building heat loss via the ground over a diurnal cycle.

The advantage of the ψ -based formulation lies in its applicability to both saturated and unsaturated soil conditions. However, as reported by several articles [9–11], it suffers poor mass balance and low convergence rate, with a consequent increase in computational effort, especially in very dry soil conditions. On the other hand, θ -based models have demonstrated significantly improved performance when applied to very dry soils, but fail in cases of layered and saturated soils [9]. Researchers have proposed various strategies to overcome these disadvantages. Celia et al. [10] and Kirkland et al. [11] suggested a mixed form of the equations, which resulted in a much improved mass balance.

All the methods used to study heat and moisture transfer in soil have been implemented using either a finite-difference or a finite-element formulation. To the authors' knowledge, the finite-volume method has not been used for this purpose. It is the intention of this work to implement the " ψ -based" [5] conservation equations in the context of a finite-volume method. As the method is inherently conservative, mass imbalance problems are not expected to arise. This will be confirmed through the test problems presented.

In the remainder of this article, the governing conservation equations and soil physical properties are briefly presented. This is followed by a description of the discretization of these conservation equations in the context of the finite-volume method, the partial elimination algorithm, and the overall solution procedure. After that, the accuracy of the newly developed numerical procedure and the correctness of its implementation are established by comparing numerical results generated for three test problems against published theoretical values.

CONSERVATION EQUATIONS OF HEAT AND MOISTURE TRANSFER IN SOIL

Almost all moisture transfer models use either the moisture content (θ -based) [3, 10] or matric potential (ψ -based) formulation [5]. The matric potential (pressure

head), ψ , is a parameter used to describe the soil water energy level, which is responsible for water movement in a soil matrix (ψ is positive for a saturated soil and negative for an unsaturated soil). To handle both saturated and layered soils, the moisture and energy conservation equations are written, in this work, in terms of matric potential (ψ) and temperature (T), respectively. Assuming an incompressible, homogeneous, nondeformable, and isotropic soil, these equations are expressed as [7, 8, 12]

$$C_{\psi\psi} \frac{\partial \psi}{\partial t} + C_{T\psi} \frac{\partial T}{\partial t} = \nabla \cdot (D_{\psi\psi} \nabla \psi) + \nabla \cdot (D_{T\psi} \nabla T) + \frac{\partial K}{\partial z}$$
(1)

$$C_{TT} \frac{\partial T}{\partial t} + C_{\psi T} \frac{\partial \psi}{\partial t} = \nabla \cdot (D_{\psi T} \nabla \psi) + \nabla \cdot (k \nabla T) + q'''$$
 (2)

where

$$C_{\psi\psi} = \frac{\varphi \rho_{vs}}{\rho_{l}} \left[\left(\frac{(\eta - \theta_{l})g}{R_{w}T} - \frac{\partial \theta_{l}}{\partial \psi} \Big|_{T} \right) \right] + \left(\frac{\partial \theta_{l}}{\partial \psi} \right)_{T} \qquad C_{TT} = C + \rho_{l} h_{fg} C_{Tv}$$

$$C_{T\psi} = \frac{\varphi \rho_{vs}}{\rho_{l}} \left[\left(\frac{(\eta - \theta_{l})}{\rho_{vs}} - \frac{\partial \theta_{l}}{\partial T} \Big|_{\psi} \right) \right] + \left(\frac{\partial \theta_{l}}{\partial T} \right)_{\psi} \qquad C_{\psi T} = \rho_{l} h_{fg} C_{\psi v}$$

$$D_{\psi\psi} = f(\theta_{l}) D_{a} \gamma \theta_{a} \frac{\rho_{vs}}{\rho_{l}} \frac{\varphi g}{R_{w}T} + K \qquad k = k^{*} + \rho_{l} h_{fg} D_{Tv}$$

$$D_{T\psi} = f(\theta_{l}) D_{a} \varphi \frac{\rho_{vs}}{\rho_{l}} \left(\frac{1}{\rho_{vs}} \frac{d\rho_{vs}}{dT} - \frac{\psi g}{R_{w}T^{2}} + \frac{g}{R_{w}T} \frac{\partial \psi}{\partial T} \Big|_{\theta} \right) \frac{(\nabla T)_{p}}{(\nabla T)} \qquad D_{\psi T} = \rho_{l} h_{fg} D_{\psi v}$$

$$(3)$$

The meanings of the variables in Eqs. (1)–(3) are as given in the Nomenclature. Equations (1) and (2) show that the ψ [Eq. (1)] and T [Eq. (2)] equations are similar except for the last term on their right-hand sides. The terms on the left-hand sides correspond to the stored mass and energy due to the temporal change in matric potential and temperature. The first two terms on the right-hand sides account for mass transfer [Eq. (1)] and heat transfer [Eq. (2)], respectively, due to moisture and temperature gradients. The last term in the first equation represents mass transferred by gravitational effects, while that in the second equation represents heat generation per unit volume. Moreover, $f(\theta_l)$ is a correction factor calculated using the expression given in Appendix I.

Equations (1)–(3) reveal the strong coupling between heat and moisture transfer in soil, the highly nonlinear nature of this coupling, and the extensive number of unknowns involved that depend heavily on the physical properties of soil. Therefore, an understanding of the various terms concerned in these equations is essential for a proper numerical implementation. In addition, estimating the thermal and hydraulic properties of soil, which are strong functions of the moisture content, is considered one of the most difficult stages in the modeling of heat and moisture transfer in soils. The correlations used for evaluating the soil water retention, hydraulic conductivity, thermal conductivity, and specific heat are briefly reviewed next.

PHYSICAL PROPERTIES OF SOIL

Moisture Retention

The moisture content is related to the matric potential (ψ) through the following analytical expression developed by Van Genuchten [13]:

$$\Theta = \frac{\theta - \theta_r}{\theta_s - \theta_r} = \left[1 + |\alpha \psi|^n\right]^{-m} \qquad m = 1 - \frac{1}{n}$$
(4)

where Θ is the degree of saturation, θ_s is water content at saturation, and α and n are empirical parameters that are assigned the values of 3.337 and 1.355, respectively, in this work [13]. Moreover, the residual water content θ_r is a fitting parameter included to achieve a better match in the low-moisture-content range. To account for the effect of temperature when calculating θ using Eq. (4), the value of ψ obtained from Eq. (1) is multiplied by the ratio of the surface tensions (σ) at a reference temperature and the temperature of interest. This results in

$$\psi(T, \theta_l) = \frac{\sigma(T)}{\sigma(T_r)} \psi(T_r, \theta_l) \qquad \sigma = 0.1171 - 1.516 * 10^{-4} T$$
 (5)

Hydraulic Conductivity

The ease with which a fluid is transported through a porous medium depends on its hydraulic conductivity. Based on Richard's law [9], which is a modified version of Darcy's law, the flow of water through unsaturated soil can be written as

$$u_l = K \nabla \Phi \tag{6}$$

where u_l is the bulk liquid velocity, Φ is the total matric potential of the soil defined as the sum of matric and gravitational potential and is taken positive upwards ($\Phi = \psi + z$), and K is the hydraulic conductivity, which is a function of soil properties, moisture content, and temperature that is given by

$$K(\theta, T) = K_s K_T(T) \Theta^{\tau} [1 - (1 - \Theta^{1/m})^m]^2$$
(7)

This equation is similar to van Genuchten's [13] model but with minor modifications to account for the effect of temperature, with τ being an empirical constant and the exponent m as defined in Eq. (4). Moreover, K_s is the hydraulic conductivity at saturation and K_T is a correction-factor function of temperature (T) and water dynamic viscosity (μ_I) given by

$$K_T(T) = \frac{\mu_l(T_o)}{\mu_l(T)} = 1.12 * 10^{-4} T^2 - 4.12 * 10^{-2} T + 3.46$$
 (8)

Thermal Conductivity

The heat flow through a soil matrix is controlled by the effective thermal conductivity k [Eq. (2)] of the system, which is mainly affected by moisture content.

An increase in the moisture content results in higher thermal conductivity. In addition, soil thermal conductivity is influenced by temperature, size, geometry, packing, and type of grains. As shown in Eq. (3), k involves two heat transfer mechanisms that are not strictly additive, but rather interactive [4], and therefore are brought into one term. Several models for computing k have been proposed, and the one adopted in this work is due to Janssen [8], which is a combination of the de Vries [14] and Campbell et al. [15] models. In this model, the effective thermal conductivity is calculated by

$$k = \frac{\sum_{i=1}^{5} \xi_i \theta_i k_i}{\sum_{i=1}^{5} \xi_i \theta_i} \tag{9}$$

In the above equation, i = 1 stands for water, 2 for trapped gases in the pores, 3 for quartz, 4 for organic material, and 5 for other minerals. The ratio of thermal gradients of component i and the medium (ξ_i) is calculated from

$$\xi_i = \frac{2}{3} \left[1 + \left(\frac{k_i}{k_m} - 1 \right) g_i \right]^{-1} + \frac{1}{3} \left[1 + \left(\frac{k_i}{k_m} - 1 \right) (1 - 2g_i) \right]^{-1}$$
 (10)

Here g_i is a shape factor that is equal to 0.144 for quartz and other minerals and 0.5 for organic materials. In addition, the thermal conductivity of the continuous medium (k_m) changes smoothly from that of air at dry condition to that of water at saturation according to

$$k_{m} = k_{a} + f_{w}(k_{w} - k_{a}) \qquad f_{w} = \left[1 + \left(\frac{\theta}{\theta_{k}}\right)^{-q}\right]^{-1} \qquad q = q_{o}\left(\frac{T}{303}\right)^{2}$$

$$k_{a} = 0.02417 + 7.596 * 10^{-5}(T - 273.15)$$

$$k_{w} = 0.5694 + 1.847 * 10^{-3}(T - 273.15) - 7.394 * 10^{-6}(T - 273.15)^{2}$$
(11)

where θ_k is the moisture content value at which water starts to be the continuous fluid, and q indicates the rapidity of this transition. Janssen [8] developed the following empirical relations for the parameters θ_k and q_o , with the sand fraction Sa as main variable:

$$\theta_k = 0.21 - 0.16 \,\text{Sa}$$
 $q_o = 4 - \text{Sa}$ (12)

Moreover, for the calculation of the shape factor of gas-filled pores, g_2 , needed in the evaluation of ξ_2 , an empirical relation is developed as [8]

$$g_2 = 0.0675 + 0.074 \,\text{Sa} \tag{13}$$

Furthermore, the thermal conductivity of the gas-filled pores, k_2 , is estimated as the sum of the thermal conductivity of air, k_a , and that of the vapor, k_v , with the

thermal conductivity of trapped vapor, following Philip and de Vries [3], assumed proportional to the relative humidity φ and given by

$$k_2 = k_a + k_v$$
 $k_v = k_{v,\text{sat}} \varphi$ $\varphi = \exp\left(\frac{\psi g}{R_w T}\right)$ $k_{v,\text{sat}} = h_{fg} D_a \frac{d\rho_{vs}}{dT}$ (14)

where h_{fg} is the latent heat of vaporization, D_a is the vapor diffusion coefficient in air, and ρ_{vs} is the saturated vapor density calculated using the expressions given in Appendix II [16].

Finally, for nearly dry soil, the thermal conductivity is calculated using the de Vries [14] equation with $\theta_1=0$, $\theta_2=\eta$ (porosity), $\xi_2=1$, and the result is multiplied by 1.25.

Specific Heat

The volumetric heat capacity (C) is calculated, neglecting the heat capacity of gases, as a weighted average of the specific heat capacities C_P of the soil constituents and is given by

$$C = \theta_w \rho_w C_{Pw} + \sum_{i}^{n} \theta_i \rho_i C_{Pi}$$
 (15)

FINITE-VOLUME FORMULATION

Because of their complexity and nonlinearity, the equations governing coupled heat and mass transfer in soil cannot be solved analytically except in very special situations. Therefore, a numerical approach is a natural alternative. The finite-volume method [17] is used in this work. The formulation starts by noticing the similarity of Eqs. (1) and (2). If the variables in these equations are denoted by $\phi^{(1)}$ and $\phi^{(2)}$, then Eq. (1) may be represented as

$$C^{\phi^{(1)}} \frac{\partial (\phi^{(1)})}{\partial t} + C^{\phi^{(12)}} \frac{\partial (\phi^{(2)})}{\partial t} = \nabla \cdot \left(\Gamma^{\phi^{(1)}} \nabla \phi^{(1)} \right) + \nabla \cdot \left(\Gamma^{\phi^{(12)}} \nabla \phi^{(2)} \right) + Q^{\phi^{(1)}}$$
(16)

where the expressions for $C^{\phi^{(1)}}$, $C^{\phi^{(12)}}$, $\Gamma^{\phi^{(12)}}$, $\Gamma^{\phi^{(12)}}$, and $Q^{\phi^{(1)}}$ can be deduced from the modeled equation. Equation (2) may be obtained from Eq. (16) by simply interchanging the superscripts (1) and (2). This general transport equation [Eq. (16)] is discretized using the finite-volume method [17]. In this approach, the solution domain is divided into a number of control volumes, each associated with a main grid point P (Figure 1a). The discretization process is a two-step procedure. In step 1, the general equation is integrated over a control volume (Figure 1a) to obtain a discretized description of the conservation law. In step 2, an interpolation profile is used to reduce the integrated equation to an algebraic equation by expressing the variation in the dependent variable and its derivatives in terms of the grid-point values [18]. Then, the set of algebraic equations is solved iteratively using the tri-diagonal matrix algorithm (TDMA) [17].

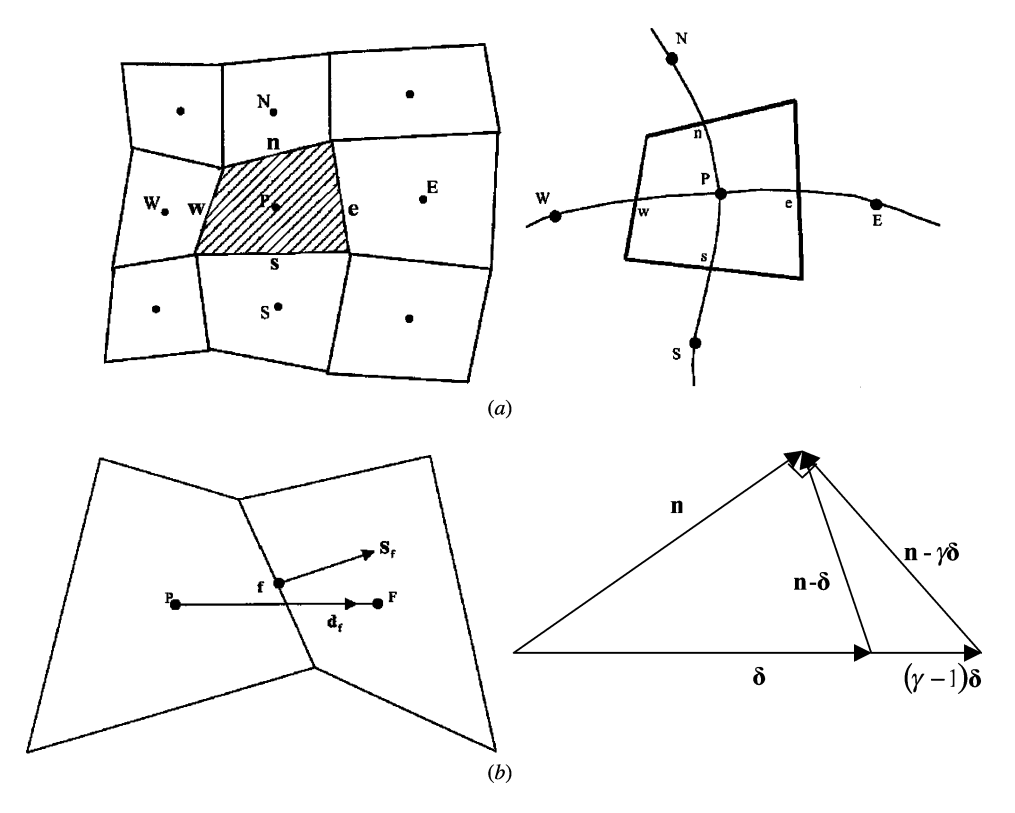


Figure 1. (a) Control volume. (b) Typical control-volume faces and geometric nomenclature.

To perform step 1, Eq. (16) is integrated over the control volume shown in Figure 1a with the flux components transformed into surface integrals. This procedure yields

$$\int_{\Omega} \left(C^{\phi^{(1)}} \frac{\partial \phi^{(1)}}{\partial t} + C^{\phi^{(12)}} \frac{\partial \phi^{(2)}}{\partial t} \right) d\Omega - \oint_{S} \left(\Gamma^{\phi^{(1)}} \nabla \phi^{(1)} + \Gamma^{\phi^{(12)}} \nabla \phi^{(2)} \right) \cdot d\mathbf{S} = \int_{\Omega} Q^{\phi^{(1)}} d\Omega \tag{17}$$

where Ω is the volume of cell P. Replacing the surface integral over the control volume by a discrete summation of the flux terms over the sides of the control volume, Eq. (17) becomes

$$\left(C^{\phi^{(1)}} \frac{\partial \phi^{(1)}}{\partial t}\right)_{P} \Omega_{P} + \left(C^{\phi^{(12)}} \frac{\partial \phi^{(2)}}{\partial t}\right)_{P} \Omega_{P}
- \sum_{f=\text{nb}(P)} \left(\Gamma^{\phi^{(1)}} \nabla \phi^{(1)} + \Gamma^{\phi^{(12)}} \nabla \phi^{(2)}\right)_{f} \cdot \mathbf{S}_{f} = Q_{P}^{\phi^{(1)}} \Omega_{P}$$
(18)

In step 2, Eq. (18) is transformed into an algebraic equation through the use of an interpolation profile, or an estimate of how ϕ varies between nodes. The approximation scheme produces an expression for the face value which is dependent on the nodal ϕ values in the vicinity of the face. For compactness, the superscripts (1) and (2) will be dropped in the derivations that follow. For the unsteady term, the use of a Euler-implicit formulation results in

$$C^{\phi} \frac{\partial(\phi)}{\partial t} = (C^{\phi})_{P} \frac{\phi_{P} - \phi_{P}^{\circ}}{\Delta t} \tag{19}$$

where Δt represents the time step and the superscript ° denotes old values obtained at time $(t - \Delta t)$. The diffusion flux is discretized along each surface of the control volume using the method described by Zwart et al. [19], according to which it is decomposed into

$$(-\Gamma^{\phi}\nabla\phi)_{f}\cdot\mathbf{S}_{f} = (-\Gamma^{\phi}\nabla\phi)_{f}\cdot\mathbf{n}_{f}S_{f} = -\Gamma^{\phi}_{f}\Big[(\nabla\phi)_{f}\cdot(\gamma\delta)_{f} + (\overline{\nabla}\overline{\phi})_{f}\cdot(n_{f} - (\gamma\delta)_{f})\Big]S_{f}$$
(20)

where $(\overline{\nabla \phi})_f$ is the average of the adjacent cell gradients, \mathbf{n}_f and $\mathbf{\delta}_f$ (Figure 1b) are the contravariant (surface vector) and covariant (curvilinear coordinate) unit vectors, respectively, and γ is a scaling factor. This factor is chosen such that it is equal to 1 on orthogonal meshes in order for the method to collapse to classical stencils. With this constraint, the expression for γ on structured meshes is given by

$$\gamma_f = \frac{1}{\mathbf{n}_f \cdot \mathbf{\delta}_f} = \frac{\mathbf{S}_f d_f}{\mathbf{S}_f \cdot \mathbf{d}_f} \tag{21}$$

Defining the space vector κ_f as

$$\kappa_f = [\mathbf{n}_f - (\gamma \mathbf{\delta})_f] S_f = \kappa_f^{\chi} \mathbf{i} + \kappa_f^{\chi} \mathbf{j}$$
 (22)

the expression for $(-\Gamma^{\phi}\nabla\phi)_f \cdot \mathbf{S}_f$ becomes

$$(-\Gamma^{\phi}\nabla\phi)_{f}\cdot\mathbf{S}_{f} = -\Gamma_{f}^{\phi}\left[(\nabla\phi)_{f}\cdot(\boldsymbol{\delta})_{f}\frac{\mathbf{S}_{f}d_{f}}{\mathbf{S}_{f}\cdot\mathbf{d}_{f}}S_{f} + (\overline{\nabla}\phi)_{f}\cdot(\kappa_{f}^{x}\mathbf{i} + \kappa_{f}^{y}\mathbf{j})\right]$$
(23)

In this form, the term $(\nabla \phi)_f \cdot (\delta)_f$ represents the gradient in the direction of the coordinate line joining P and F (see Figure 1b). Therefore, the above equation can be rewritten as

$$(-\Gamma^{\phi}\nabla\phi)_{f}\cdot\mathbf{S}_{f} = -\Gamma_{f}^{\phi}\left[(\phi_{F} - \phi_{P})\frac{\mathbf{S}_{f}\cdot\mathbf{S}_{f}}{\mathbf{S}_{f}\cdot\mathbf{d}_{f}} + (\overline{\nabla}\phi)_{f}\cdot(\kappa_{f}^{x}\mathbf{i} + \kappa_{f}^{y}\mathbf{j})\right]$$
(24)

The interpolated gradient at the interface $(\overline{\nabla \phi})_f$ is calculated as

$$(\overline{\nabla \phi})_f = f_f(\nabla \phi)_P + (1 - f_f)(\nabla \phi)_F \tag{25}$$

and the gradient at the main grid point F (F = P, E, W, N, or S) is obtained from

$$(\nabla \Phi)_F = \frac{1}{\Omega} \int_{\Omega} \nabla \Phi \, d\Omega = \frac{1}{\Omega} \oint_{S} \Phi \, dS = \frac{1}{\Omega} \sum_{f = \mathsf{nb}(F)} \Phi_f \mathbf{S}_f \tag{26}$$

The final form of the diffusive flux along face f (f = e, w, n, or s) is given by

$$(-\Gamma^{\phi}\nabla\phi)_{f} \cdot \mathbf{S}_{f} = -\Gamma_{f}^{\phi}(\phi_{F} - \phi_{P}) \frac{(S_{f}^{x})^{2} + (S_{f}^{y})^{2}}{S_{f}^{x}d_{f}^{x} + S_{f}^{y}d_{f}^{y}}$$

$$-\frac{\Gamma_{f}^{\phi}\left\{\left[f_{f}(\nabla\phi)_{P}^{x} + (1 - f_{f})(\nabla\phi)_{F}^{x}\right]\kappa_{f}^{x} + \left[f_{f}(\nabla\phi)_{P}^{y} + (1 - f_{f})(\nabla\phi)_{F}^{y}\right]\kappa_{f}^{y}\right\}}{(27)}$$

The underlined part of the diffusion flux is called the cross-diffusion contribution. It vanishes when the grid is orthogonal, and is small compared to normal diffusion for a nearly orthogonal grid. In such circumstances, explicit treatment of the cross-diffusion term does not significantly influence the rate of convergence of the overall solution procedure and simplifies the matrix of coefficients.

The integral value of the source term over the control volume P (Figure 1a) is obtained by assuming the estimate of the source at the control-volume center to represent the mean value over the whole control volume. Hence, one can write

$$\int_{\Omega} Q^{\phi} d\Omega = Q_P^{\phi} \Omega_P \tag{28}$$

To increase the robustness of the numerical method, the source term is linearized according to [17]

$$(Q_P^{\phi})^n = (Q_P^{\phi})_C + (Q_P^{\phi})_P \phi_P = (Q_P^{\phi})^{n-1} + \left(\frac{\partial Q^{\phi}}{\partial \phi}\right)^{n-1} (\phi_P - \phi_P^{n-1})$$
(29)

where $(Q_P^{\phi})_P$ should always be a negative quantity. The diffusion term involving $\phi^{(2)}$ appearing in the $\phi^{(1)}$ equation is treated explicitly, and its discretization is analogous to that of the ordinary diffusion flux.

The discretized equation [Eq. (18)] is transformed into an algebraic equation at the main grid point P by substituting the fluxes at all faces of the control volume by their equivalent expressions. Then, performing some algebraic manipulations on the resultant equation, the following algebraic relation, linking the value of the dependent variable at the control-volume center to the neighboring values, is obtained:

$$a_P^{\phi^{(1)}} \phi_P^{(1)} + a_P^{\phi^{(12)}} \phi_P^{(2)} = \sum_{F = NB(P)} a_F^{\phi^{(1)}} \phi_F^{(1)} + b_P^{\phi^{(1)}}$$
(30a)

where

$$a_{P}^{\phi^{(1)}} = \left(a_{P}^{\phi^{(1)}}\right)^{t} + \left(a_{P}^{\phi^{(1)}}\right)^{D} - \left(Q_{P}^{\phi^{(1)}}\right)_{P}^{D} \Omega_{P} \qquad a_{P}^{\phi^{(1)}} = \left(a_{P}^{\phi^{(2)}}\right)^{t} + \left(a_{P}^{\phi^{(2)}}\right)^{D}$$

$$a_{F}^{\phi^{(1)}} = \left(a_{F}^{\phi^{(1)}}\right)^{D} = \Gamma_{f}^{\phi^{(1)}} \frac{\left(S_{f}^{x}\right)^{2} + \left(S_{f}^{y}\right)^{2}}{S_{f}^{x} d_{f}^{x} + S_{f}^{y} d_{f}^{y}} \qquad \left(a_{P}^{\phi^{(1)}}\right)^{D} = \sum_{F=NB(P)} \left(a_{F}^{\phi^{(1)}}\right)^{D}$$

$$a_{F}^{\phi^{(2)}} = \left(a_{F}^{\phi^{(2)}}\right)^{D} = \Gamma_{f}^{\phi^{(1)}} \frac{\left(S_{f}^{x}\right)^{2} + \left(S_{f}^{y}\right)^{2}}{S_{f}^{x} d_{f}^{x} + S_{f}^{y} d_{f}^{y}} \qquad \left(a_{P}^{\phi^{(2)}}\right)^{D} = \sum_{F=NB(P)} \left(a_{F}^{\phi^{(2)}}\right)^{D}$$

$$\left(a_{P}^{\phi^{(1)}}\right)^{t} = \frac{\left(C^{\phi^{(1)}}\right)_{P} \Omega_{P}}{\Delta t} \qquad \left(a_{P}^{\phi^{(2)}}\right)^{t} = \frac{\left(C^{\phi^{(12)}}\right)_{P} \Omega_{P}}{\Delta t}$$

$$b_{P}^{\phi^{(1)}} = \sum_{F=NB(P)} \left(a_{F}^{\phi^{(2)}}\right)^{D} \phi_{F}^{(2)} + \left(Q_{C}^{\phi^{(1)}}\right)_{P} \Omega_{P} + \left(a_{P}^{\phi^{(1)}}\right)^{t} \left(\phi_{P}^{(1)}\right)^{0} + \left(a_{P}^{\phi^{(2)}}\right)^{t} \left(\phi_{P}^{(2)}\right)^{0}$$

$$+ \sum_{f=nb(P)} \Gamma_{f}^{\phi^{(1)}} \left\{ \left[f_{f} \left(\nabla \phi^{(1)}\right)_{P}^{x} + (1 - f_{f}) \left(\nabla \phi^{(1)}\right)_{F}^{x}\right] \kappa_{f}^{x} + \left[f_{f} \left(\nabla \phi^{(2)}\right)_{P}^{x} + (1 - f_{f}) \left(\nabla \phi^{(2)}\right)_{F}^{x}\right] \kappa_{f}^{y} \right\}$$

$$+ \sum_{f=nb(P)} \Gamma_{f}^{\phi^{(12)}} \left\{ \left[f_{f} \left(\nabla \phi^{(2)}\right)_{P}^{x} + (1 - f_{f}) \left(\nabla \phi^{(2)}\right)_{F}^{x}\right] \kappa_{f}^{y} + \left[f_{f} \left(\nabla \phi^{(2)}\right)_{P}^{x} + (1 - f_{f}) \left(\nabla \phi^{(2)}\right)_{F}^{y}\right] \kappa_{f}^{y} \right\}$$

where the superscripts t and D indicate coefficients obtained from the discretization of the transient term and of the diffusion fluxes, respectively, and the superscript $^{\circ}$ designates a value from the previous time step. Using Eq. (30), the algebraic forms of Eqs. (1) and (2) are given by

$$a_{P}^{\psi}\psi_{P} + a_{P}^{\psi T}T_{P} = \sum_{F = NB(P)} a_{F}^{\psi}\psi_{F} + b_{P}^{\psi}$$

$$a_{P}^{T}T_{P} + a_{P}^{T\psi}\psi_{P} = \sum_{F = NB(P)} a_{F}^{T}T_{F} + b_{P}^{T}$$
(31)

The terms with cross coefficients (i.e., $a_P^{\Psi T} T_P$ and $a_P^{T\Psi} \psi_P$) are evaluated explicitly, because the adopted procedure is iterative. This practice increases the value of the source term and slows down the rate of convergence. The procedure can be rendered more implicit by decoupling the two sets of equations, by eliminating, for example, the variable T_P from the ψ_P equation, and vice versa, as is done in a two-phase flow through the partial elimination algorithm (PEA) [20]. This is achieved in a straightforward algebraic manner and results in a modification to

the values of the coefficients. The equations resulting after this partial elimination are written as

$$\frac{a_{P}^{\psi}a_{P}^{T} - a_{P}^{\psi T}a_{P}^{T\psi}}{a_{P}^{T}}\psi_{P} = \sum_{F=NB(P)} a_{F}^{\psi}\psi_{F} + b_{P}^{\psi} - \frac{a_{P}^{\psi T}}{a_{P}^{T}} \left(\sum_{F=NB(P)} a_{F}^{T}T_{F} + b_{P}^{T} \right)
\frac{a_{P}^{\psi}a_{P}^{T} - a_{P}^{\psi T}a_{P}^{T\psi}}{a_{P}^{\psi}} T_{P} = \sum_{F=NB(P)} a_{F}^{T}T_{F} + b_{P}^{T} - \frac{a_{P}^{T\psi}}{a_{P}^{\psi}} \left(\sum_{F=NB(P)} a_{F}^{\psi}\psi_{F} + b_{P}^{\psi} \right)$$
(32)

This partial elimination makes the equations more implicit (T_P is absent from the ψ_P equation and vice versa) and enhances the robustness of the iterative procedure. Letting ϕ denotes either ψ or T, the above system of equations can again be expressed as

$$A_P^{\phi} \phi_P = \sum_{F = \text{NB}(P)} A_F^{\phi} \phi_F + B_P^{\phi} \tag{33}$$

Since the procedure is iterative in nature, the equations are usually underrelaxed [17, 18]. Denoting the underrelaxation factor by α , Eq. (33) becomes

$$\left(\frac{A_P^{\phi}}{\alpha}\right) \phi_P = \sum_{F = NB(P)} A_F^{\phi} \phi_F + B_P^{\phi} + \frac{(1 - \alpha)}{\alpha} A_P^{\phi} \phi_P^{n-1} \tag{34}$$

where the superscript (n-1) refers to values taken from the previous iteration. This equation can again be rewritten as

$$\mathbf{A}_{P}^{\phi}\phi_{P} = \sum_{F=\mathrm{NB}(P)} \mathbf{A}_{F}^{\phi}\phi_{F} + \mathbf{B}_{P}^{\phi} \tag{35}$$

For every variable ϕ , an algebraic equation similar to Eq. (35) is obtained at the geometric center of each control volume in the computational domain, and the collection of these equations forms a system that is solved using a line-by-line Thomas algorithm [17] to arrive at the solution. Since the coefficients are highly nonlinear and interdependent, an iterative approach is adopted and is summarized as follows:

- 1. Start with an initial guess for T and ψ at the current time.
- 2. Use available values of T and ψ to calculate the physical properties of soil needed in the equations.
- 3. Calculate the coefficients of the *T* equation.
- 4. Calculate the coefficients of the ψ equation.
- 5. Perform partial elimination to calculate the new coefficients for the ψ and T equations, underrelax the equations, and solve them.
- 6. Repeat steps 2–5 until a converged solution at the current time is obtained.
- 7. Move in time and repeat steps 1–6 until solutions over the entire desired time period are found.

RESULTS AND DISCUSSION

The numerical method presented above is used for predicting moisture and temperature distributions in soil. To assure correctness and accuracy, verification is performed by solving several test problems of increasing complexity and comparing the results against available theoretical values. Because the equations of coupled heat and mass transfer are nonlinear, analytical solutions for the entire set of equations are currently not available. As a result, different problems are used to test different features of the numerical model.

First, a solution for dry soil is carried out to assure that the unsteady heat conduction equation is working properly. Second, the infiltration of liquid moisture in soil is tested using the semianalytical solution of Philips [21]. Finally, the analytical solution of Crank [22] is used to test the coupled diffusion of heat and water vapor in dry soil, which also serves as a good test for the mass imbalance problem faced by several workers [10, 11] using either the finite-difference or finite-element method.

Test 1: Temperature Distribution in Dry Soil

A soil column of depth 2 m, density $2,000 \,\mathrm{kg/m^3}$, thermal conductivity $2.511 \,\mathrm{W/m}\,\mathrm{K}$, heat capacity $837.2 \,\mathrm{J/kg}\,\mathrm{K}$, and initial uniform temperature $293 \,\mathrm{K}$ is used in this test. The surface temperature of the soil is raised at time t=0 to $310 \,\mathrm{K}$ and the numerical method developed is used to predict the temperature distribution in the soil after 1, 4, 9, 16, and 25 h. The results obtained are compared to the analytical solution of unsteady conduction in a semi-infinite wall [23], assuming that heat flows in the vertical direction only. As shown in Figure 2, the numerical code accurately reproduces the results of the analytical solution, with predictions being in excellent agreement with analytical values. This is an indication of the correct implementation of the unsteady and conduction terms in the energy equation.

Test 2: Moisture Distribution in Isothermal Soil

This is a benchmark quasi-analytical solution developed by Philip [21] to test the isothermal infiltration of liquid moisture in soil. Neglecting the vapor and thermal effects, the governing equation in one dimension is written as [21]

$$\left(\frac{\partial \theta}{\partial \psi}\right) \frac{\partial \psi}{\partial t} = \frac{\partial}{\partial z} \left(K \frac{\partial \psi}{\partial z}\right) + \frac{\partial K}{\partial z} \tag{36}$$

where the boundary conditions assigned for this problem are as follows:

$$\psi(0,z) = -600 \,\text{cm}$$
 $\psi(t,0) = 0 \,\text{cm}$ $\psi(t,-40 \,\text{cm}) = -600 \,\text{cm}$ (37)

A Yolo light clay soil is used whose correlations have been fitted by Haverkamp et al. [24]. The moisture retention curve and the relative hydraulic

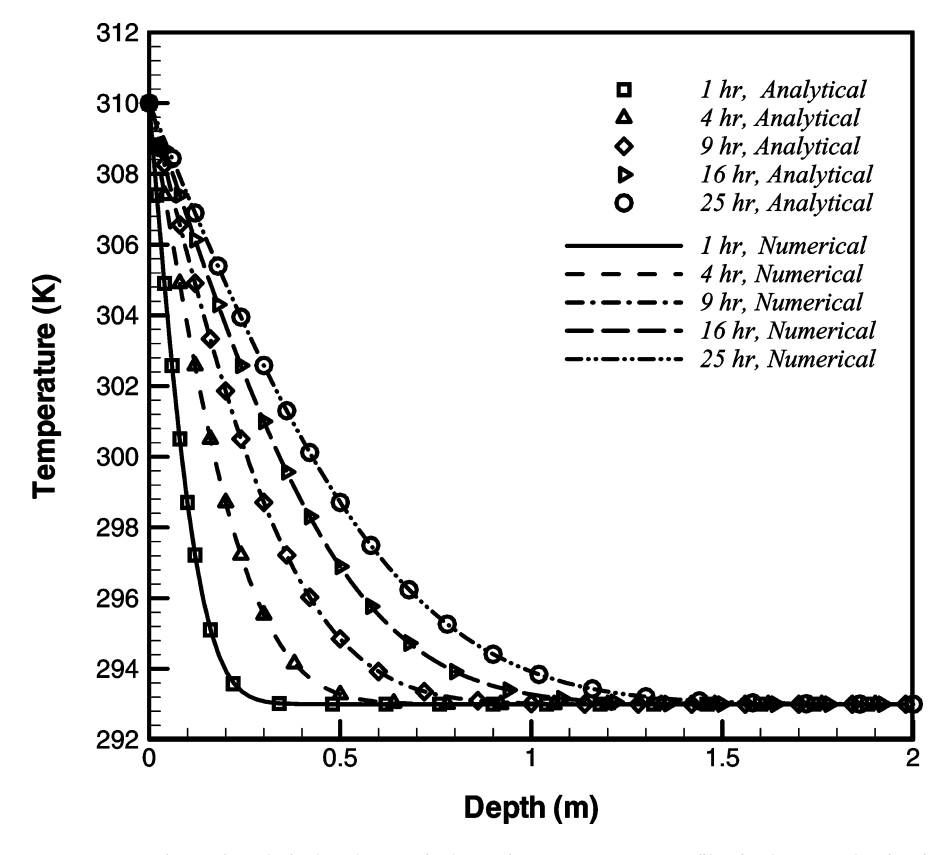


Figure 2. Comparison of analytical and numerical transient temperature profiles for heat conduction in a semi-infinite column of dry soil.

conductivity are given by

$$\theta = \begin{cases} 0.124 + \frac{274.2}{739 + [\ln(-\psi)]^4} & \psi < -1 \text{ cm} \\ 0.495 & \psi \ge -1 \text{ cm} \end{cases}$$

$$K = K_s \frac{124.6}{124.6 + (-\psi)^4} \qquad K_s = 1.27*10^{-5} \text{ cm/s}$$
(38)

A column of height 0.4 m is used to simulate the semi-infinite medium considered by Philip [21]. The distribution of moisture content versus depth is shown in Figure 3 at the following times: 10^3 , 10^4 , 4×10^4 , and 10^5 s. The time step used in the simulation is 1 s during the first 10^3 s, and 10-50 s afterwards.

A simple modification of this problem is done by assuming that water is impounded at the surface, in which case $\psi(t,0\,\mathrm{cm})=25\,\mathrm{cm}$. The current numerical solution for this problem [generated using Eq. (2)], along with that developed by

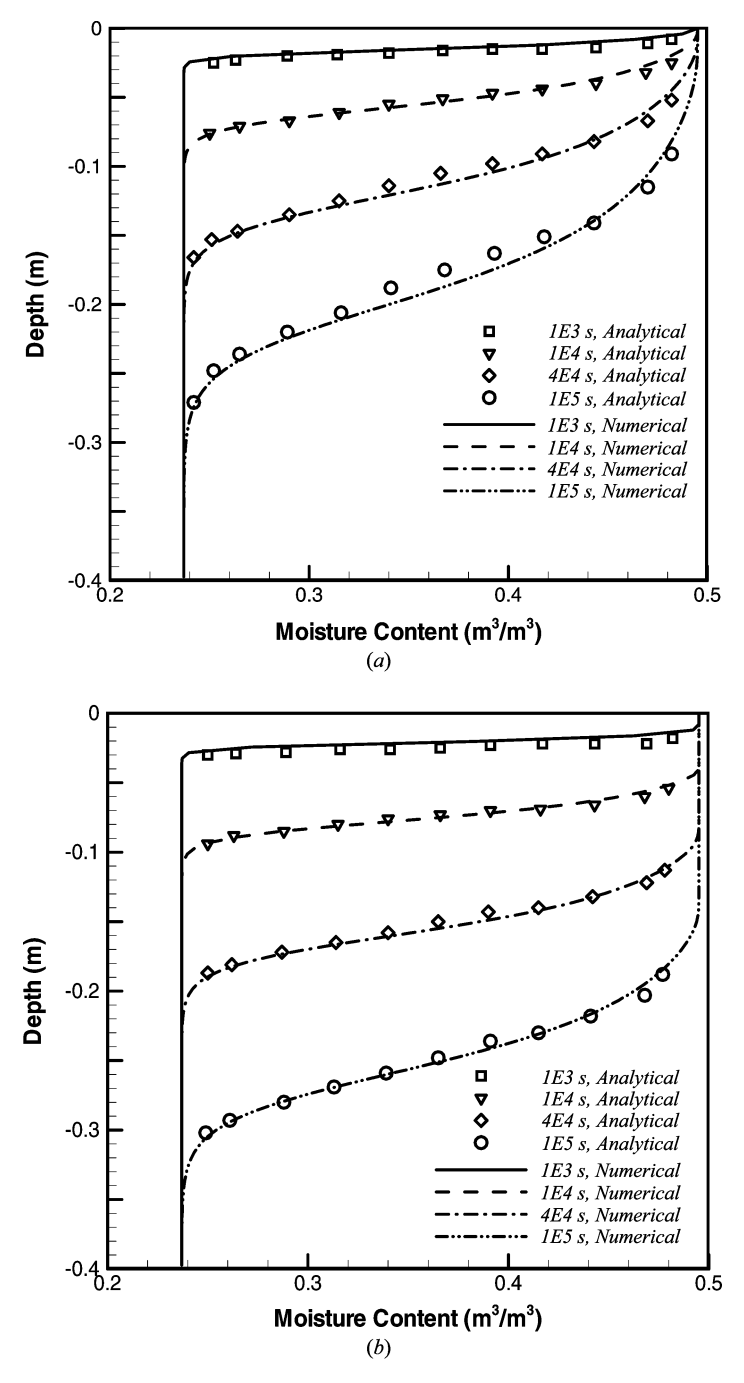


Figure 3. Infiltration of moisture into Yolo light clay with (a) zero and (b) 25-cm matric potential at the surface predicted analytically and numerically.

Philip [21], are shown in Figures 3a and 3b. Both figures show that the current numerical solution accurately predicts the quasi-analytical solution of the problems. This is an indication of the correct implementation of the unsteady, conduction, and matric potential gradient terms in the moisture conservation equation.

Test 3: Coupled Heat and Water Vapor Diffusion

This situation, which is used to test the coupling between the heat and mass conservation equations, represents an initially very dry soil column subjected to a sudden increase in vapor density at one end; this is equivalent to a sudden increase in matric potential, while the temperature is unchanged. The other end of the soil column is assumed to be fully adiabatic and impermeable to heat and moisture flow. The vapor, as a result, diffuses into the column, condenses, and releases heat, resulting in a temporary rise in soil temperature that will return to its original value as the vapor diffuses out of the column. An analytical solution for this problem is possible subject to the following simplifications:

The correction factors ξ and $f(\theta)$ are set to unity.

The flow of liquid is negligible.

The sensible heat carried by the flow of water vapor is negligible.

Heat and mass transfer equations are linearized around the basic state, because the changes in temperature and vapor density are small.

The values of all properties are assumed to be constant and equal to their initial value.

With the above assumptions, the heat and mass transfer equations reduce to

$$C\frac{\partial T}{\partial t} - \rho_l h_{fg} \frac{\partial \theta_l}{\partial t} = \nabla \cdot \left\{ \left[k - D_a \gamma (\eta - \theta_l) \frac{\partial \rho_v}{\partial T} \right] \nabla T \right\}$$

$$(\eta - \theta_l) \frac{\partial \rho_v}{\partial t} + (\rho_l - \rho_v) \frac{\partial \theta_l}{\partial t} = \nabla \cdot \left[D_a \gamma (\eta - \theta_l) \nabla \rho_v \right]$$
(39)

Crank [22] developed an analytical solution for this problem by converting Eqs. (39) into a pair of independent diffusion equations using a dependent-variable transformation.

A 10-cm long Yolo light clay column initially maintained at a temperature of 293.15 K and a matric potential of -2×10^4 m is employed to simulate the problem numerically. For this value of ψ , the soil is very dry. Therefore, this situation represents an extreme case for testing the mass balance problem suffered by the ψ -based formulation [10] when implemented using a finite-element or a finite-difference numerical method. The matric potential at the top boundary is suddenly increased to -1.8×10^4 m. Setting the thermal conductivity and the heat capacity of the soil to 1.5 W/m K and $2 \times 10^6 \text{ J/m}^3 \text{ K}$, respectively, and neglecting the effect of hydraulic conductivity, the change in vapor density and temperature are computed numerically

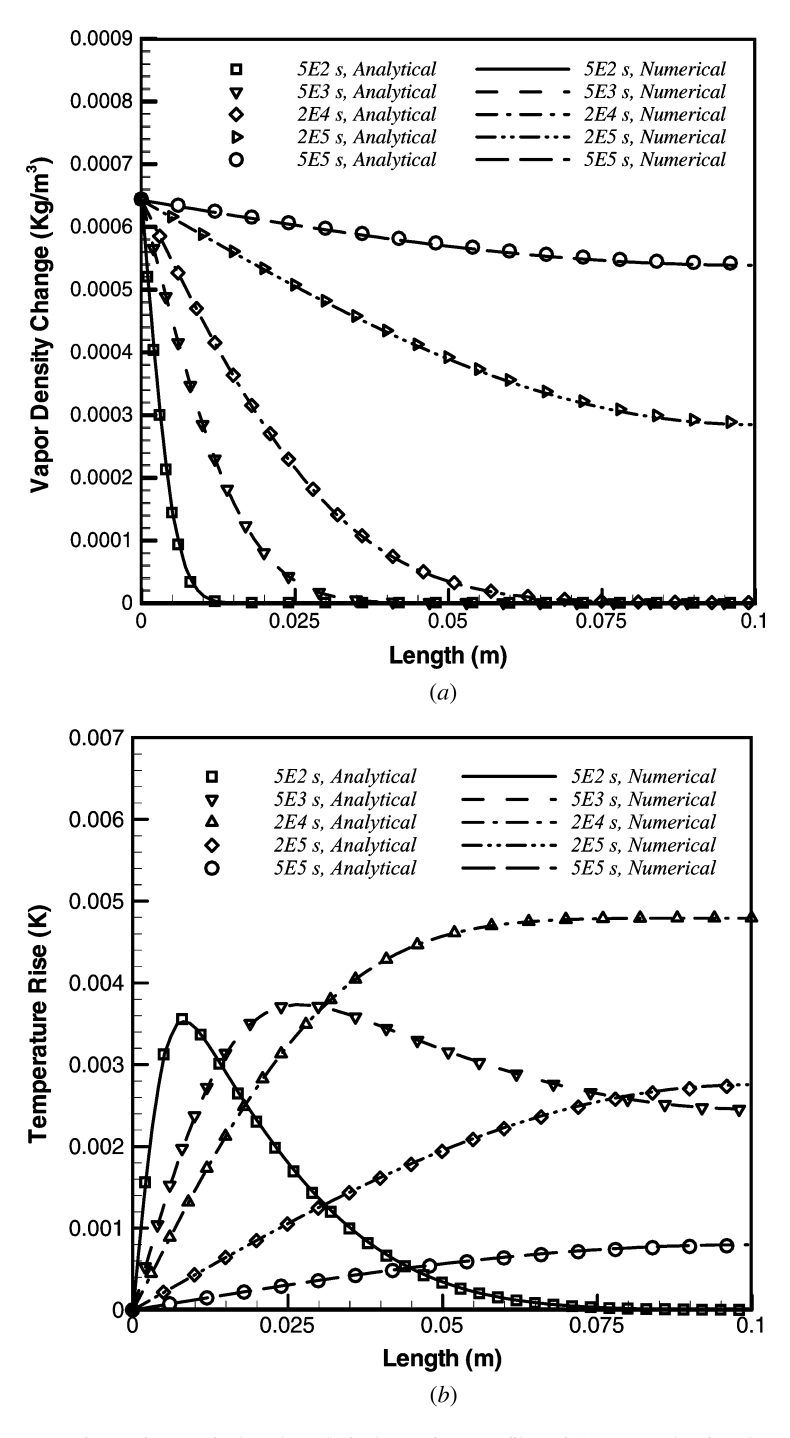


Figure 4. Comparison of numerical and analytical transient profiles of (a) vapor density change and (b) temperature rise in soil for the coupled heat and water vapor diffusion problem.

by solving Eqs. (1) and (2). Results are displayed in the form of change in vapor density and temperature profiles in Figures 4a and 4b, respectively, at the following times: 500, 5,000, 2×10^4 , 2×10^5 , and 5×10^5 s. As depicted, numerical and analytical results are identical, indicating the correctness of the numerical implementation of all terms involved in the coupled equations. More important, the results reveal that even for a very dry soil, the ψ -based formulation does not suffer a conservation (mass imbalance) problem when implemented in the context of a finite-volume numerical method.

CLOSING REMARKS

A finite-volume method for predicting unsteady heat and moisture transfer in soil was presented and tested. The heat and moisture equations were written with temperature and matric potential as the dependent variables. To increase implicitness and improve robustness, the iterative solution procedure was implemented within a partial elimination algorithm. The accuracy of the model was verified by solving three problems involving transfer of heat in a dry soil, transfer of moisture in an isothermal soil, and coupled heat and water vapor diffusion in soil. Numerical results were found to be in excellent agreement with analytical values.

REFERENCES

- 1. F. Moukalled, N. Ghaddar, Y. Saleh, and Z. Fawaz, Heat and Mass Transfer in Moist Soil, Part II. Application to Predicting Thermal Signatures of Buried Landmines, *Numer. Heat Transfer B, Fundamentals*, vol. 49, pp. 487–512, 2006.
- 2. S. A. Taylor and J. W. Cary, Linear Equations for Simultaneous Flow of Water and Energy in Continuous Soil System, *Soil Sci. Soc. Am. J.*, vol. 28, pp. 167–172, 1964.
- 3. J. R. Philip and D. A. De Vries, Moisture Movement in Porous Materials under Temperature Gradients, *Trans. Am. Geophys. Union*, vol. 38, no. 2, pp. 222–232, 1957.
- 4. D. A. De Vries, Simultaneous Transfer of Heat and Moisture in Porous Media, *Trans. Am. Geophys. Union*, vol. 39, no. 5, pp. 909–915, 1958.
- 5. P. C. D. Milly, Moisture and Heat Transport in Hysteretic, Inhomogeneous Porous Media: A Matric Head-Based Formulation and a Numerical Model, *Water Resources Res.*, vol. 18, no. 3, pp. 489–498, 1982.
- 6. M. Sophocleous, Analysis of Water and Heat Flow in Unsaturated-Saturated Porous Media, *Water Resources Res.*, vol. 15, pp. 1195–1206, 1979.
- 7. M. Deru, A Model for Ground-Coupled Heat and Moisture Transfer from Buildings, Natl. Renewable Energy Lab. Tech. Rep. NREL/TP-550-33954, June 2003.
- 8. H. Janssen, The Influence of Soil Moisture Transfer on Building Heat Loss via the Ground, Ph.D. thesis, Katholieke Universiteit Leuven, Leuven, Belgium, 2002.
- 9. D. Hillel, Environmental Soil Physics, Academic Press, San Diego, CA, 1998.
- M. Celia, A. Efthimios, T. Bouloutas, and R. L. Zarba, A General Mass-Conservative Numerical Solution for the Unsaturated Flow Equation, *Water Resources Res.*, vol. 23, pp. 1483–1496, 1990.
- 11. M. R. Kirkland, R. G. Hills, and P. J. Wierenga, Algorithms for Solving Richards' Equation for Variably Saturated Soils, *Water Resources Res.*, vol. 28, pp. 2049–2058, 1992.

- 12. P. C. D. Milly, Mass-Conservative Procedure for Time-Stepping in Models of Unsaturated Flow, *Adv. Water Resources*, vol. 8, no. 1, pp. 32–36, 1985.
- 13. M. T. Van Genuchten, Closed-Form Equation for Predicting the Hydraulic Conductivity of Unsaturated Soils, *Soil Sci. Soc. Am. J.*, vol. 44, no. 5, pp. 892–898, 1980.
- 14. D. A. De Vries, Thermal Properties of Soils, in W. R. van Wijk (ed.), *Physics of Plant Environment*, pp. 210–235, Amsterdam, North-Holland, 1963.
- G. S. Campbell, J. D. Jungbauer, W. R. Bidlake, and R. D. Hungerford, Predicting the Effect of Temperature on Soil Thermal Conductivity, *Soil Sci.*, vol. 158, pp. 307–313, 1994.
- 16. 2001 ASHRAE Handbook, Fundamentals, American Society of Heating, Refrigerating and Air-Conditioning Engineers, Atlanta, GA, 2001.
- 17. S. V. Patankar, *Numerical Heat Transfer and Fluid Flow*, Hemisphere, McGraw-Hill, Washington, DC, New York, 1980.
- 18. F. Moukalled and M. Darwish, A Unified Formulation of the Segregated Class of Algorithms for Fluid Flow at All Speeds, *Numer. Heat Transfer B*, vol. 37, pp. 103–139, 2000.
- 19. P. J. Zwart, G. D. Raithby, and M. J. Raw, Integrated Space-Time Finite-Volume Method For Moving-Boundary Problems, *Numer. Heat Transfer B*, vol. 34, no. 3, pp. 257–270, 1998.
- D. B. Spalding and N. C. Markatos, Computer Simulation of Multi-phase Flows: A Course of Lectures and Computer Workshops, Rep. CFD/83/4, Mech. Eng., Imperial College, London, 1983.
- 21. J. R. Philip, The Theory of Infiltration: 1. The infiltration Equation and Its Solution, *Soil Sci.*, vol. 83, pp. 435–448, 1957.
- 22. J. Crank, The Mathematics of Diffusion, Clarendon Press, Oxford, UK, 1956.
- 23. F. P. Incropera and D. P. DeWitt, *Fundamentals of Heat and Mass Transfer*, Wiley, New York, 2002.
- R. Haverkamp, M. Vauclin, J. Touma, P. J. Wierenga, and G. Vachaud, Comparison of Numerical Simulation Models for One-Dimensional Infiltration, *Soil Sci. Soc. Am. J.*, vol. 41, no. 2, pp. 285–294, 1977.

APPENDIX I

The correction factor $f(\theta_l)$ needed in Eq. (3) was introduced by Philip and de Vries [3] to account for the liquid water islands that are present in the soil, which act as a shortcut for vapor transfer, thus enlarging the cross section available for vapor transport. Philip and de Vries [3] suggested the following equation to compute $f(\theta_l)$:

$$f(\theta_{l}) = \eta \qquad \text{for } \theta_{l} \leq \theta_{k}$$

$$= (\eta - \theta_{l}) + \frac{\theta_{l}(\eta - \theta_{l})}{(\eta - \theta_{k})} \qquad \text{for } \theta_{l} > \theta_{k}$$
(AI-1)

in which the porosity η is assumed equal to the saturated volumetric moisture content θ_s , and θ_k is the critical moisture content below which liquid is no longer the continuous medium.

APPENDIX II

Estimates for the latent heat of vaporization h_{fg} , the vapor diffusion coefficient in air D_a , and the saturated vapor density ρ_{vs} needed in Eq. (14) are computed using the following expressions [17]:

$$h_{fg} = 2.445 * 10^{6} - 2130(T - 293.15) \qquad D_{a} = 2.17 * 10^{-5} \left(\frac{T}{273.15}\right)^{1.88}$$

$$\begin{cases} \rho_{vs} = \exp\left(\frac{13.873T - 3529.9}{T - 105.84}\right) * 10^{-3} & T > 273.15 \end{cases}$$

$$\begin{cases} \rho_{vs} = \frac{1,000}{461.5T} \exp\left[\frac{c_{1}}{T} + c_{2} + c_{3}T + c_{4}T^{2} + c_{5}T^{4} + c_{6}T^{4} + c_{7}\ln(T)\right] & T \leq 273.15 \end{cases}$$

$$c_{1} = -5674.5359 \qquad c_{2} = 0.51523058 \qquad c_{3} = -9.677843 * 10^{-3}$$

$$c_{4} = 6.2215701 * 10^{-3} \qquad c_{5} = 2.0747825 * 10^{-9} \qquad c_{6} = -9.484024 * 10^{-13}$$

$$c_{7} = 4.1635019 \qquad (AII-1)$$